Dear Prof. Zhang,

Thank you for giving us the opportunity to submit a revised version of the manuscript titled "Experimental analysis of a horizontal axis wind turbine with swept blades using PIV data" to *Wind Energy Science*. We appreciate the time and effort that you and the reviewers have dedicated to providing valuable feedback on our manuscript. We have been able to incorporate changes to reflect the suggestions provided by the reviewers. Please find a point-by-point response to their comments below.

Reviewer 1: Dr. Alessandro Fontanella

1. As a general comment, I would like to see (at the beginning of the methodology or in the introduction) an explanation of what is expected to happen in a swept blade from the aerodynamic point of view, especially if compared to a straight blade. Authors decided to measure and present in the article some quantities (velocities, flow angles, section loads) and I ask them to explain why these quantities are important to study (e.g., because they see a significant change passing from a straight blade to swept blade, or because they are difficult to predict with current engineering models for rotor aerodynamics, . . .).
Thank you for this comment. Previous numerical investigations have shown that blade aerodynamics are affected by sweep. In particular, sweep leads to a misalignment between the airfoil orientation and the local inflow in the swept part of the blade. Additionally, the trailed vorticity system is displaced in azimuthal direction, and the now curved bound vortex (thinking in lifting line terms) induces a velocity on itself. The relevance of the experimental dataset presented in this study then lies in enabling the validation of numerical models in terms of quantities such as induction, flow angles and blade loads. We have added this line of argumentation in the introduction section, see Page 2, Line 44.

2. The scale model blades show small pitch offsets and a bend-twist coupled elastic response. At line 146 it is said that blades were designed to be stiff, thus I suppose that the bend-twist deformation is unwanted, but it seems to affect results. I ask authors to clarify this aspect and explain which effects in the results are wanted and which are not, but are a consequence of manufacturing difficulties (that I think are normal at this scale).
You are right, the bend twist coupling was unintended but does affect the results. We have clarified our motivation to built stiff blades in the description of the scaled model, see Page 4, Line 85. Furthermore, we confirm that it is indeed challenging to discern between the purely aerodynamic effects of blade sweep and the additional changes in local aerodynamics due to the aeroelastic blade response, see Page 12, Line 236. We'd be happy to hear about your experience with these challenges at a given opportunity.

3. "Such values would be unrealistic on a full-scale, operational wind turbine". Can you provide typical values for an operational wind turbine?
We have added a reference to the STAR project, see Page 3, Line 67, which is the only publicly reported research project on a full-scale wind turbine with swept blades. Here, blades with 8 %R tip sweep were tested in the field. It should be noted, that this experiment was conducted on a sub-megawatt rotor with a tip radius of 28 m. In unpublished work, the authors have investigated swept blade designs for a multi-megawatt machine. From this work, it seems more realistic that swept blades would have a tip sweep below 5 %R on modern wind turbines.

4. "To maintain the same tip radius as the unswept reference blade, the swept blade axis coordinates are scaled by. . . ". I think this is not clear. You should explain what happens if you do not scale the blade axis coordinates.
Thank you for pointing out that this needs further clarification. The scaling of the blade axis coordinates is applied to ensure that both sets of blades have identical blade tip radii and, thus, also rotor disc areas. We have added an additional sentence to clarify this, see Page 3, Line 74.

5. "was mounted rigidly on a traversing system". I suppose the traversing system moves the PIV plane in a radial direction. Please add this information for clarity.
We have adjusted the text to be specify the movement direction, see Page 5, Line 109.

6. Figure 4. This figure is not explained clearly. Please explain the difference between the green shape and the blue shape. The meaning of the different line styles is explained in the figure caption. I think it would be better to explain it inside the figure with a legend.
   We can see how this was not entirely clear and have made adjustments aligned with your suggestions. We hope that the new version of Figure 4 is more intuitive.

7. *Additional comment from the technical correction attachment referring to line 114 (in the original submission):* What is the implication of this distortion? A few lines before, you said that measurements are set up to have comparisons with a straight blade. Is it possible to make comparisons if the PIV plane is not aligned with the airfoil?
   Upon rereading this section, we feel the two sentences at the end of this subsection add more confusion than that they are useful. We have removed them, see Page 6, Line 132. The implication of the misalignment of airfoil orientation and measurement plane is that care needs to be taken in the analysis of the derived quantities. The forces and induction terms are defined in the two directions that span the measurement plane. Thus, no special treatment of the derived values is needed here. The inflow angle and the angle of attack, however, are defined in the plane of the airfoil orientation and are, thus, a function of the global and local sweep angles, see Equation (4).

8. 122-124. It seems contradictory that you remove the induction and then you compute the induction. I suggest explaining briefly how the method works.
   We have adjusted the text, see Page 7, Line 141, and hope this makes it clearer. The method only removes the local induction due to the blade cross-section. After this removal, the flow field is the sum of the freestream velocity vector and the velocities induced by the remainder of the blades and the wake. This yields the relative inflow vector and, consequently, the induction terms, inflow angle and angle of attack.

9. Do you have an explanation on why the Noca's method does not work for tangential force? Maybe it is worth to report the KJ's and Noca's methods in the article appendix and use the appendix to explain where the Noca's method fails.
   The wind tunnel model runs at a fairly high tip speed ratio and has low torque and tangential force values. It is our understanding that it is very difficult to capture the change in momentum associated with this small tangential force using Noca's method. We have added this information to the text, see Page 8, Line 150. Your suggestion regarding an appendix to discuss this in more detail has already been implemented in our paper on the straight-bladed reference experiment (https://doi.org/10.5194/wes-9-1173-2024). To avoid the reporting of an essentially identical analysis, we have added another reference to this paper in the text so that an interested reader will easily find it.

10. Add a short introduction at the beginning of the Results section where you explain the content of the next subsections.
    We have added an introduction to the Results section, see Page 8, Line 173.

11. "The blades used in this experiment were manually manufactured. . . ". I suggest moving this sentence in section 2.1. The orientation of fibers plays a role in the bend-twist coupling of blades.
    We agree that it makes sense to move this sentence to the Methodology section. It is now placed at Page 4, Line 85.

12. Explain if this was controlled in the manufacturing process and if you expect it to influence the results.
    We could indeed see minor changes in the fibre orientation which were cause by the resin pushing through the layup during the infusion process. We have added a statement along those lines, see Page 8, Line 175.

13. 152-158. Please explain why you correct the airfoil to align it to the illuminated cross section.
    The illuminated cross-section represents the blade shape during operation. The overlaid red shape is the original design and, thus, the expected airfoil orientation. The green airfoil shape is obtained by applying a rotation until it better aligns with the illuminated cross-section. The rotation angle between the red and green shapes then corresponds to a deviation from the original blade twist distribution and pitch angle. We have made changes to the paragraphs you indicate and hope that this clarifies our motivation for this approach. Maybe we misunderstand where the confusion came from. If so, we would be happy to answer additional comments.

14. 163-164. "All three blades exhibit twisting behaviour...". This is measured by the variation of DeltaBeta between at the blade tip and root. DeltaBeta at r/R = 0 is instead the blade pitch offset (right?)
    Yes, this is indeed correct. We tried to express this with the term $\Delta\beta_{tip-root}$, but we can see that we can still be more precise. We have altered this term to $\Delta\beta(r = R) - \Delta\beta(r = 0)$, see Page 10, Line 200.

15. Table 3. I suggest putting the equations in the text and avoid the use of a table.
    We have replaced the table with equations, see Page 10, Line 210.

16. "Non-dimensionalized". How did you normalize measurements? Can you recall how you computed Vrel?
    The velocity fields are non-dimensionalised using the local relative inflow velocity V_{rel} for which we have now added the equation here, rather than later in the text, as was the case in the original manuscript, see Page 10, Line 214.

17. Figure 7. I suggest to add in the figure a line for reference straight blades.
    We would like to refrain from including the data from the straight-bladed campaign here for two reasons. Firstly, we see the experiment with swept blades as an independent study and we want to analyse the data of both experiments individually before drawing any comparisons in potential future work. Secondly, the straight blades also suffered from pitch offsets and minor twist deformations. Thus, a fair comparison of the straight and swept blade data cannot be ensured without further analyses that we consider outside the scope of this paper. We hope you can agree with our line of argumentation to leave this figure as is.

18. "where the twist deformations vary strongly" and where measurements are more uncertain due to the small dimensions of the airfoil?
    We don't think the small dimension of the airfoil necessarily introduces higher uncertainties. If that would be the case, this increased uncertainty would also show up in the error bars. We hope you can agree with our decision to not alter this section of the manuscript.

19. 209-210. "This corresponds to the forces in the coordinate system spanning the measurement planes...". Add a reference to Fig. 4 if you think it's useful
    Thank you for this suggestion. We have added the reference, see Page 14, Line 256.

Next to these specific comments, the technical corrections suggested in the attachment to your comment have been included in the manuscript. Thank you for the precise and detailed review!

Reviewer 2

1. Overall, I found section 2.2 confusing. It gives a lot of information very densely and it is hard to understand the experimental setup properties. First, as other referee remarked, figure 4 is nor properly explained. Furthermore, I find the perspective of the laser sheet from figure 3 ambiguous, and it does not allow to see the field of view extend and direction.
   In line with your comment and that of reviewer 1, we have made adjustments to Figure 4, which hopefully improve its clarity. We have also added a short explanation of the updated figure, see Page 6, Line 123. Regarding the perspective of the laser sheet, we have added a clarification of its orientation to the caption of Figure 3 to avoid any confusion.

2. I understand the difficulty in explaining the very large amount of SPIV planes covered, but in its present state the reader requires some time to understand them (for example, the so-called blade 1 was tested in 22 planes while 2 and 3 were tested in only 4). The authors may consider adding an extra table better detailing such measurements. I also propose that the laser planes are defined in terms of fixed cartesian coordinates instead of relatively to the blades.
   Thank you for this suggestion. We have added a table more clearly defining the measurement planes in Appendix B and a reference to this appendix in the text, see Page 5, Line 117.

3. Connected to my previous comment, if the authors have a film of the experimental setup running, that can bed added to the public dataset, may help to support section 2.2.

Unfortunately, we do not have a video of the setup running with the laser sheet visible. We will, however, check whether any other media material we collected could help in the understanding of the experimental setup and upload it to the dataset.

4. I also agree with another reviewer about adding to the manuscript which parameters from equation 1 correspond to a realistic shape. While I understand the authors plan to do a further manuscript in this topic, the present work would greatly benefit from testing the BEM correction model for swept blades (Fritz et al. (2022)) to test the sensibility of the lift coefficient from the blade to the parameters from equation 1.
Regarding the realistic values, please refer to our answer to comment 3 of reviewer 1. Regarding testing the sensibility of the lift coefficient, I am not sure I fully understand your comment. In case you mean a sensitivity study of how blade aerodynamics change with different sweep parameters, I would like to refer your to the original publication of the sweep correction model (Fritz et al. (2022)), where we simulated different swept blade configurations. In case you meant a validation of the sweep correction model using the experimental data: We have submitted a paper for the Torque 2024 conference dealing with this, which I hope would then answer your comment. In either case, we think it is best to retain a single focus for the present paper (the presentation of the experimental data) instead of mixing experimental and numerical work. We hope you can agree with this opinion.

5. Related to the last comment, the authors say in line 147: 'Experience from previous experiments taught that the stiffness properties of the three blades can vary considerably'. How much they change? Furthermore, figures 10 and 11 show significant differences in terms of performance between blades. A sensitivity analysis would help to see if this is indeed due to the manufacturing of the current blades or an actual limitation for the application of swept blades in wind energy.
Upon rereading this section, we realise that the sentence you refer to is misleading. We never actually measured stiffness properties and can, therefore, also not quantify their change. What we intended to say was that also with the straight-bladed experiment, differences in torsion deformation were observed. Looking at this section now, we see that referring back to the straight-bladed experiment has little added value since we focus on the pitch and twist offsets of the swept blades here. To avoid confusion, we have decided to remove this sentence, see Page 9, Line 181.
Regarding the second part of your comment: Twist deformations are not a limitation of swept blades but their motivation. The idea is that blade sweep couples bending and torsion deformations and, as such, can serve as a passive load alleviation technique. In the context of this experiment, we wanted to avoid these deformations since we were aiming to isolate aerodynamic rather than aeroelastic effects. In my opinion, a sensitivity analysis would require manufacturing a larger number of blades than the three we have now and then doing a dedicated analysis of their structural properties. While this would be a valuable exercise and would help to produce more consistent experimental results in the future, we consider this outside of the scope of this work.

6. 120 phase-locked images were recorded at each plane to extract the average velocity field and its standard deviation. Can the authors comment about the convergence of the fields?
As also indicated by the very narrow confidence interval present in Figures 7 – 10, the phase-locking worked very well, and the flow conditions were steady. To corroborate this, we checked the convergence of e.g. the circulation value derived from the flow field for varying numbers of PIV images used in the averaging process. The result is shown for three radial locations in Figure 0 as a function of a number of randomly selected images. It is evident that even with much smaller numbers than the total acquired 120 images, a converged result can be obtained.

7. Why figures 2 and 3 do not expand the full range of the blade (0<r/R<1)?
The blade root radius is $r_{root} = 0.06\,\mathrm{m} = 0.0667\,\mathrm{R}$ and, therefore, an extension of the blade axis, chord distribution and twist distribution as shown in those figures to $r/R = 0$ would not be realistic. I have clarified this, see Page 3, Line 74.

8. While they can be deduced from available data, the Reynolds number of the blades and rotor should be better specified.
Thanks for this comment. A similar comment was also made in the review of the paper presenting the data from the straight-bladed experiment, which was ongoing in parallel (https://doi.org/10.5194/wes-9-1173-2024l). Therefore, we have adjusted this paper in the same fashion as we did there, see the changes made to Section 3.4. This section now also

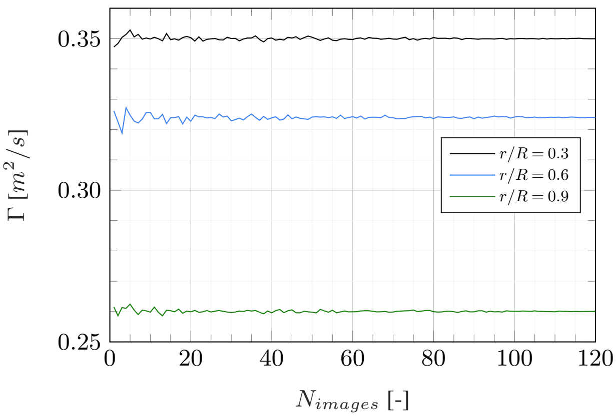

Figure 0. Convergence of the circulation as a function of the number of PIV images used for averaging

presents the chord Reynolds number distribution and an evaluation of the blade lift generation compared to the values based on the design airfoil polars.

9. In line 82, the term ’three-dimensional velocity field’ is confusing. It is the stitching process, detailed later, that allows to reconstruct three dimensional vector fields in space.
You are right, this is misleading. Thank you for pointing this out. What we meant to say was that the stereoscopic PIV setup allows the measurement of all three spatial velocity components. We have adjusted the sentence accordingly, see Page 4, Line 96.

10. The DOI towards the dataset is the manuscript is outdated (a v1 is missing).
The 4TU.ResearchData repository reserves multiple DOIs. Each dataset receives one DOI per version and one that always points to the latest version of this dataset. That is the one currently included in the manuscript. Since the dataset has not been altered since the initial upload, the given DOI as well as the one including ".v1" lead to the same data. Should the dataset be updated, the DOI given in this paper would lead to the newer dataset, which we consider to be preferable.

11. In figure 6, the velocity V and the relative velocity V_{rel} are not defined appropriately (the reader has to go to subsequent sections to find definitions).
Thank you for pointing this out. We now define the relative velocity here, see Page 10, Line 214, rather than in the lift polar section.

12. Do figures 5 and 7 have error bars? It looks like they are within the markers. If that is the case, it should be mention it in the captions.
You are right, the error bars are within the marker for most measurements (with the exception of the planes close to the blade root). Rather than mentioning this in each individual caption of Figures 7 to 10, we felt this clarification better placed at the beginning of Section 3.3, see Page 12, Line 231. We hope you agree with this assessment.

13. The phrase from line 45 ’ By basing the scaled blade geometry on the aerodynamic characteristics of the IEA 15 MW reference wind turbine (Gaertner et al., 2020), relevance for state-of-the-art wind turbine designs is ensured’, could be better sustained.
The largest commercial turbines currently built are in the range of 14-16 MW, hence this statement. However, to underline its relevance, we have reformulated this sentence, focussing more on the importance this RWT has in the scientific community. We reference to the IEA task 47, see Page 2, Line 51, in which many research organisations study the IEA 15 MW RWT to gain better insights into its aerodynamics.

We would like to thank the reviewers for their detailed and constructive feedback. Their comments have been very helpful in improving the quality of our manuscript. Please find attached a version of our manuscript highlighting all the changes made. We look forward to hearing from you in due time regarding our submission and to responding to any further questions and comments you may have.

Sincerely,
Erik Fritz, Koen Boorsma, Carlos Ferreira

Experimental analysis of a horizontal axis wind turbine with swept blades using PIV data

Erik Fritz[1,2], Koen Boorsma[1], and Carlos Ferreira[2]

[1]Wind Energy, TNO Energy Transition, Petten, Netherlands

[2]Faculty of Aerospace Engineering, Technical University of Delft, Delft, Netherlands

Correspondence: Erik Fritz (e.fritz@tno.nl)

Abstract. This study presents findings from a wind tunnel experiment investigating a model wind turbine equipped with aft-swept blades. Utilising Particle Image Velocimetry, velocity fields were measured at multiple radial stations. These allow the derivation of blade-level aerodynamic parameters, including bound circulation, induction values, inflow angle, angle of attack, and forces normal and tangential to the rotor plane. The measured local lift coefficient aligns well with the lift polar of the design airfoil, validating the experimental approach.

The resulting public dataset provides a comprehensive aerodynamic characterisation of rotating swept blades in controlled conditions. It can serve as a baseline for future experimental research on swept wind turbine blades. Furthermore, it is valuable in validating numerical models of varying fidelity simulating swept wind turbine blades. The provided blade-level aerodynamics are particularly relevant to lower fidelity models such as blade element momentum theory and lifting line algorithms. At the same time, the measured flow fields can be compared against higher fidelity simulation results from computational fluid dynamics.

1 Introduction

In the pursuit of reducing the levelised cost of energy, wind turbine rotors are becoming increasingly large. Current state-of-the-art horizontal axis wind turbines (HAWT) feature blade lengths beyond the 100 m mark. Consequently, these blades become more slender and flexible, increasing the interaction between aerodynamic forces and structural deformations. A challenge arising from this is the development of techniques which can be used to tailor the aeroelastic behaviour of blades.

Blade sweep, first discussed in the context of wind turbine blades by Liebst (1986), offers such aeroelastic tailoring potential. It is defined as the displacement of the blade axis in the rotor plane. This ~~shift of the blade axis away from the blade's pitching axis~~ [EF]creates an offset between a blade cross-section's aerodynamic and shear centre, thus coupling bending and torsional deformations. Blade sweep is, therefore, also referred to as geometric bend-twist-coupling. For example, an aft-swept blade under flapwise loading will locally twist to lower angles of attack, thereby reducing the flapwise loading (Larwood and Zuteck, 2006). The potential for bending load reduction has been demonstrated numerically by Verelst and Larsen (2010) and Larwood et al. (2014).

Conversely, this reduction in loading suggests that the diameter of a rotor with swept blades can be increased, effectively increasing the turbine's power rating, while staying within the load envelope of a straight-bladed reference rotor. This was demonstrated experimentally in the STAR (Sweep Twist Adaptive Rotor) project on a sub-megawatt wind turbine where the swept blade configuration produced $10-12\,\%$ more energy than the straight baseline configuration, see Ashwill et al. (2010).

It should be noted that blade sweep generally entails an increase in torsional moment. Numerical simulations by Verelst and Larsen (2010) and Suzuki et al. (2011) indicate this increase to be in the range of $280-400\,\%$. Another obstacle in developing swept blades on the state-of-the-art scale is that wind turbine blade design optimisation still largely relies on simulation tools based on blade element momentum theory (BEM). Its rapid calculation speed makes it the only viable tool to simulate the many load cases wind turbines experience during their lifetime in a reasonable time. BEM algorithms, in their basic form, however, cannot accurately represent the aerodynamics of swept blades as they inherently assume a straight blade geometry.

Recently, research efforts have been made to develop computationally efficient simulation tools that can account for blade sweep. Li et al. (2018, 2020, 2021) extended the near wake model by Pirrung et al. (2016) to swept blade applications. Fritz et al. (2022) present a correction model which enables BEM algorithms to account for blade sweep.

In parallel to the numerical developments, further experimental studies have been conducted. Barlas et al. (2021, 2022) tested a non-rotating[EF] swept wind turbine blade[EF] tip ~~in wing configuration~~[EF] in a wind tunnel and later on a rotor test rig in the field, which allowed the testing of the tip on a "one-armed" turbine. An experimental study of swept blades on a three-bladed rotor in controlled conditions is yet missing in the literature.

The present work provides precisely that: a~~A~~[EF] wind tunnel campaign on a HAWT equipped with swept blades. Particle Image Velocimetry (PIV) is used to measure detailed flow fields in the vicinity of the blades. Blade-level aerodynamics are derived from these flow fields, characterising the blades in terms of circulation, axial and tangential induction, inflow angle and angle of attack, and forces normal and tangential to the rotor plane. Previous studies have demonstrated that the spanwise distributions of blade-level aerodynamic quantities change with respect to a straight reference when applying blade sweep (Li et al., 2021; Fritz et al., 2022). These changes can be explained by the misalignment between the local inflow and the airfoil orientation in the swept part of the blade, the displacement of the trailed vorticity in azimuthal direction, and the induction of the curved bound vorticity on itself. The experimental dataset presented in this study enables the validation of low to high-fidelity numerical tools used for simulating the aerodynamics of swept blades in terms of the aforementioned quantities.~~As such, the created dataset is suited for the validation of low to high-fidelity numerical tools.~~[EF] By basing the scaled blade geometry on the aerodynamic characteristics of the IEA 15 MW reference wind turbine (Gaertner et al., 2020), relevance for current research interests of the wind energy community is ensured. For example, this reference turbine is being studied extensively in the ongoing IEA task 47 (Schepers, 2021).~~relevance for state-of-the-art wind turbine designs is ensured.~~[EF]

This article is structured as follows: Section 2 introduces the experimental setup, including the scaled wind turbine model and the measurement system. Furthermore, a brief description of the methods used to derive aerodynamic quantities from the PIV-processed velocity fields is given. The results are presented in Section 3. Initially, the procedure of accounting for pitch and twist deviations from the original design is explained. This is followed by analysing the flow fields, blade-level aerodynamics and the lift polar. In Section 4, conclusions are drawn, and suggestions for future research are made.

2 Methodology

2.1 Scaled wind turbine model

The wind tunnel model used for this study is a horizontal axis wind turbine with a rotor diameter of $D = 1.8\,m$. It is, with the exception of blade sweep, identical to that presented in Fritz et al. (2024). The swept blades are derived from the straight reference blade by gradually displacing the blade axis in the rotor plane as a function of the radial position r

$$y_\Lambda = \begin{cases} 0 & \text{for } r \leq r_{start} \\ y_{tip}\left(\frac{r - r_{start}}{R - r_{start}}\right)^\gamma & \text{for } r > r_{start} \end{cases} \tag{1}$$

where R is the blade tip radius. The sweep starting position is chosen as $r_{start} = 0.5\,R$, the tip displacement as $y_{tip} = 0.2\,R$ and the sweep exponent as $\gamma = 2$. Such tip displacement[EF] values would likely[EF] be unrealistic on a full-scale, operational wind turbine. For example, the blades tested in the STAR project had a tip radius of 28 m and a tip displacement of 2.2 m, corresponding to $y_{tip} = 0.08\,R$ (Ashwill et al., 2010).[EF] Nevertheless, this tip sweep is~~they are~~[EF] chosen to exaggerate the effect of sweep on the blade's aerodynamic characteristics. This exaggeration is intended to ensure that the effect of sweep exceeds the uncertainties and noise otherwise present in experimental data and, thus, facilitate the validation of numerical models. The local sweep angle can be determined as $\Lambda = \tan^{-1}(\partial y / \partial r)$. The swept blade geometry is generated by locally orienting the airfoils perpendicular to the swept blade axis. To maintain the same tip radius as the unswept reference blade, the swept blade axis coordinates are scaled by $r/\sqrt{r^2 + y_\Lambda^2}$. If this were not done, the swept blade tip radius would be $\sqrt{R^2 + y_{tip}^2}$, and the rotor area of the straight and swept blades would be unequal.[EF] The swept blade axis is depicted in Figure 1. Note that the blade root radius is $r_{root} = 0.06\,\text{m} = 0.0667\,\text{R}$.[EF]

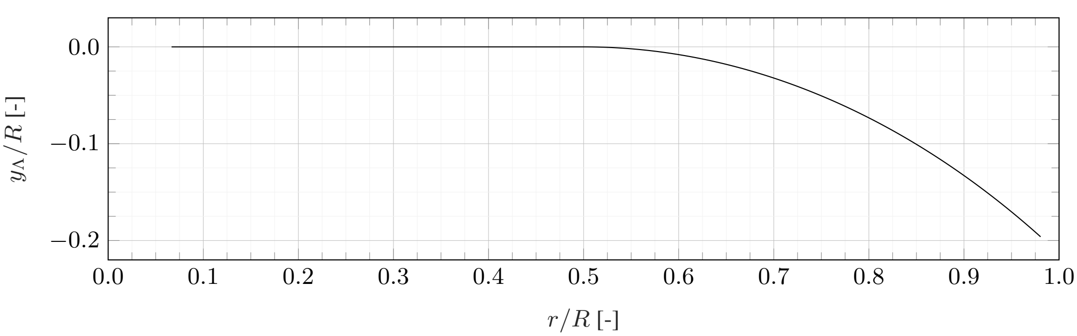

Figure 1. Swept blade axis

Chord and twist distribution of the straight reference blade, as shown in Figure 2, are kept identical for the swept blade. These distributions were derived to obtain a scaled version of the IEA 15 MW RWT as defined by Gaertner et al. (2020). The main objective of the scaling procedure was to maintain the IEA 15 MW RWT blade's non-dimensionalised thrust distribution. The blade geometry is defined by the *SD7032* airfoil, which blends into a cylinder close to the blade root. This airfoil has been used in multiple wind tunnel experiments on rotating wind turbines, e.g. by Fontanella et al. (2022) or Kimball et al. (2022), because of its good performance in low Reynolds number conditions. Details of the scaling approach can be found in Fritz et al. (2024).

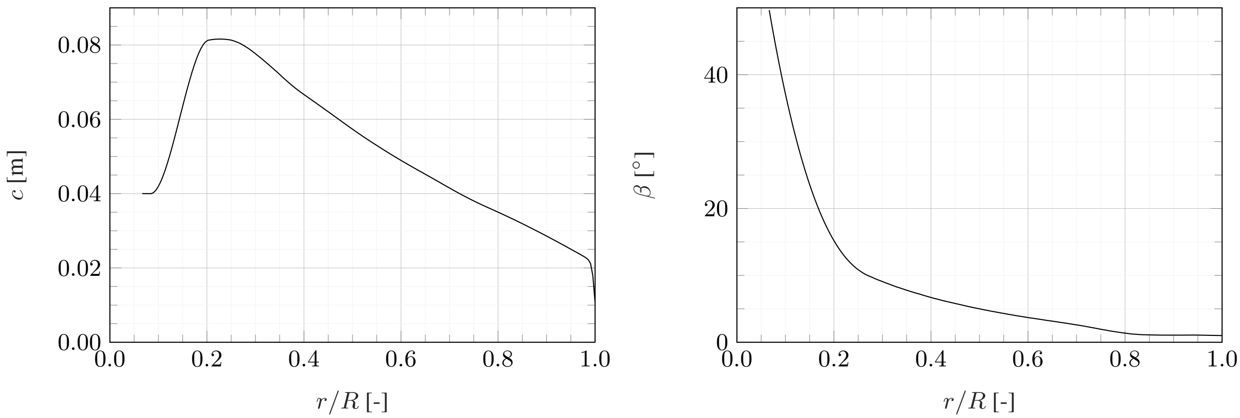

(a) (b)

Figure 2. Chord (a) and twist (b) distribution of the wind tunnel model

The blades used in this experiment were manually manufactured out of vacuum-infused carbon fibre-reinforced material. They were manufactured to be stiff to enable a purely aerodynamic analysis of blade sweep. Despite these intentions, deformations occurred, which will be discussed in more detail in Section 3.1.[EF]

2.2 Experimental setup and measurement system

The experimental campaign was conducted in TU Delft's Open Jet Facility (OJF), which has an octagonal jet exit of $2.85\,\mathrm{m}\times 2.85\,\mathrm{m}$. The model turbine was operated at a constant tip speed ratio of $\lambda = 9$ and an inflow velocity of $U_\infty = 3.95\,\mathrm{m/s}$. To exclude external phenomena from impacting the measurements, the wind tunnel's operating conditions were logged in terms of velocity, pressure, temperature and density for each measurement point and showed no significant variation (generally, less than 1 % maximum deviation from the mean value of the entire campaign).

The primary data gathered in this campaign are flow fields measured around various blade cross-sections along the span using stereoscopic particle image velocimetry (SPIV). Employing laser optics, a thin, uniform light sheet was created within a vertical measurement plane aligned with the inflow. Smoke particles were introduced into the wind tunnel downstream of the measurement section. The smoke is then distributed homogeneously during the recirculation, enabling the airflow's visualisation. Two cameras captured the flow field from two angles, allowing the measurement of velocity components in three spatial directions~~enabling the reconstruction of the three-dimensional velocity field~~[EF]. The entire flow field surrounding a blade cross-section was captured in two steps because the blade itself casts[EF] a shadow and covered part of the measurement plane from the cameras' perspective. Thus, the flow around the blade's pressure side was evaluated with the measurement setup placed upwind of the rotor and the laser sheet angled downstream. The suction side's flow was then captured by placing the apparatus downstream of the turbine and tilting the laser sheet upstream. By stitching the two measurements together in post-processing, the entire flow field was made available. This process was facilitated by the constant wind turbine [EF]operational conditions[EF] and environmental conditions of the wind tunnel.

Laser and cameras were triggered by a notch on the turbine's main shaft, activating an optical sensor once per revolution. Per measurement plane, 120 phase-locked images were recorded and post-processed into an average velocity field and its standard deviation using LaVision Davis software. While Table 1 lists more specific information regarding the hardware used in this measurement campaign, Table 2 details the SPIV measurement specifications. Figure 3 (a) shows the swept blades and Figure 3 (b) shows the wind tunnel setup and measurement system.

Illumination	Quantel Evergreen double-pulsed Neodymium-doped Yttrium Aluminium Garnet (Nd:YAG)
Seeding	Safex smoke generator, median particle diameter of 1 µm
Imaging	2 LaVision Imager sCMOS cameras with lenses of 105 mm focal length and an aperture of $f/8$
Trigger	Optical gate activated once per revolution
Computing	Acquisition PC with LaVision Davis 8 software

Table 1. Hardware used in the SPIV setup

Laser pulse time separation	150 µs
Equivalent change of turbine azimuth	$0.3\,^\circ$
Approximate particle movement	5 px
No. of phase-locked image pairs	120
Field of view	$297\,\text{mm} \times 257\,\text{mm}$
Image resolution	8.81 px/mm

Table 2. SPIV specifications

The entire SPIV setup was mounted rigidly on a traverse system moving in radial direction[EF], allowing for time-efficient measurements without the need to recalibrate the software at each new location. In total, measurements were taken at 22 planes along the blade span with the following spacing:

- $\Delta r/R = 0.100$ for $0.10 \leq r/R \leq 0.40$
- $\Delta r/R = 0.050$ for $0.40 \leq r/R \leq 0.80$
- $\Delta r/R = 0.025$ for $0.80 \leq r/R \leq 1.05$

These planes were chosen to guarantee higher resolution in the tip region where higher gradients in aerodynamic quantities and the main impact of blade sweep are expected. To evaluate how representative the main measurement blade is for the remaining two blades, measurements were taken for all three blades at $r/R = [0.4,\ 0.6,\ 0.8,\ 0.9]$. An overview of the individual measurement planes and their coordinates is given in Appendix B.[EF]

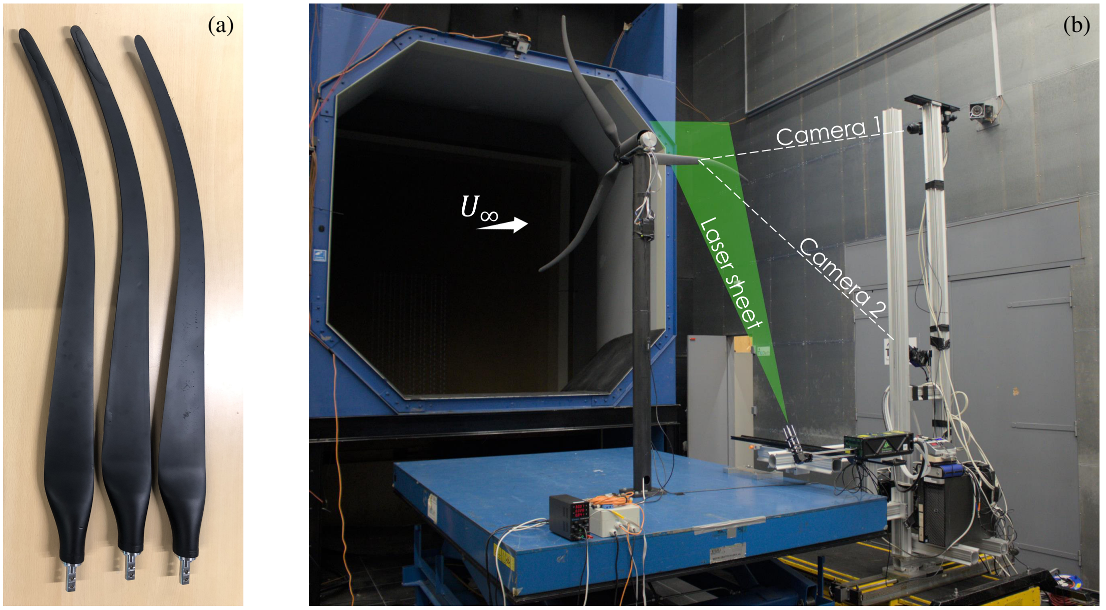

Figure 3. Swept model wind turbine blades (a) and experimental setup and measurement system (b), the laser sheet is oriented in the plane spanned by the vertical and the inflow direction[EF]

A time delay was set between the trigger signal and camera/laser activation for measurement planes in the swept part of the blade. This is to ensure that (1) the blade cross-section remains in the centre of the FOV and (2) that the radial position of the measurements is equivalent to the measurements on the straight reference blades as presented by Fritz et al. (2024). This increases the comparability of the two wind tunnel campaigns. Figure 4 shows a supporting schematic of this approach. Figure 4 (a) is representative for measurements in the unswept part of the blade. Here, the measurement plane is perpendicular to the blade axis. Figure 4 (b) is representative of measurements in the swept part of the blade, where the local blade axis is not perpendicular to the measurement plane.[EF] Two coordinate systems are introduced: o~~O~~[EF]ne global coordinate system and one aligned with the local blade axis and airfoil orientation. In the unswept part of the blade, these two coordinate systems coincide.

The global sweep angle of a given blade section[EF] ζ and the required additional time delay Δt_Λ are calculated as

$$\zeta = \tan^{-1}\left(\frac{y_\Lambda}{r}\right) \tag{2}$$

$$\Delta t_\Lambda = \frac{\zeta}{\omega} \tag{3}$$

where ω is the angular velocity.

~~As can be seen from Figure 4, measurement planes in the swept part of the blade are not aligned with the local airfoil orientation. Therefore, the cross-section around which the flow is captured is not represented by the original *SD7032* airfoil but by a version scaled in the chordwise direction by $1/\cos(\Lambda-\zeta)$.~~[EF]

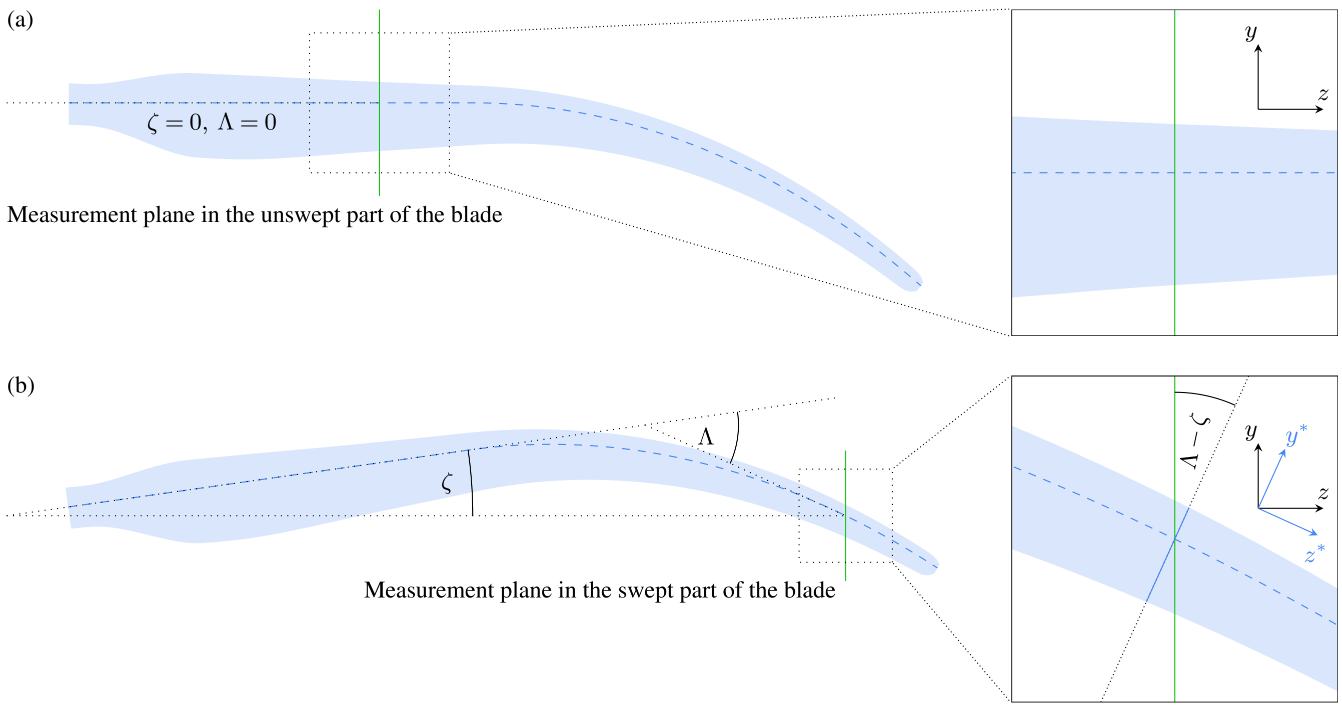

Figure 4. Schematic of measurement planes in the unswept (a)~~(black, dashed)~~[EF] and swept (b)~~(black, solid)~~[EF] part of the blade~~; zoom shows the airfoil orientation (blue, solid) in the swept part of the blade and the two coordinate systems~~[EF]

2.3 Deriving blade level aerodynamics from PIV measurements

In this study, multiple aerodynamic quantities are derived from the measured flow fields. Only a brief summary of the methods employed is given here. For a detailed description and the mathematical formulation of these methods, the reader is referred to Fritz et al. (2024).

All methods rely on evaluating the velocity field on a closed curve encompassing the investigated blade cross-section. The bound circulation Γ is computed as the line integral of the measured velocity field along this control curve (e.g. Anderson, 2017, p. 176). The inflow conditions are determined using the Ferreira-Micallef approach (Rahimi et al., 2018). It aims to remove the regarded blade cross-section's induction from the measured flow field using elemental potential flow solutions. What is left after this removal is the sum of the freestream velocity and the velocities induced by the remainder of the blades and the wake, yielding the relative inflow vector.~~It aims to remove the blade induction from the measured flow field using elemental potential flow solutions, yielding the relative inflow vector.~~[EF] The inflow vector then allows the computation of induction values, inflow angle and angle of attack. The blade forces are calculated using two approaches, namely Noca's method (Noca et al., 1999), which calculates the forces using a momentum balance based on the velocity field along a control volume's bounding curve,[EF] and the Kutta-Joukowski theorem, which directly relates the forces to the bound circulation (e.g. Anderson, 2017, p. 282).

It was found that Noca's method is only reliable when determining the normal force. In contrast, the tangential force did not converge for varying control volume sizes. The developed wind tunnel model turbine has low torque and tangential force values. Consequently, accurately capturing the momentum change associated with the tangential force proves challenging when utilising the Noca method.[EF] The same challenge was observed by Fritz et al. (2024), and the reader is referred to this work for a more detailed discussion[EF]. Given this challenge~~Therefore~~[EF], only the tangential force based on the Kutta-Joukowski theorem is presented in this article. It should be noted that the Kutta-Joukowski theorem is based on potential flow theory, thus it ~~and, thus,~~[EF] neglects the viscous drag contribution to the tangential force. While this might lead to some inaccuracies in the tangential force, the neglection of viscosity has limited impact on the normal force.

As discussed in Section 2.2, the airfoil orientation and measurement plane do not align in the swept part of the blade. Therefore, additional considerations are necessary. Firstly, the inflow angle in the measurement plane and the inflow angle in the plane perpendicular to the local blade axis differ. The rotational velocity needs to be decomposed and only its component aligned with the airfoil orientation should be considered in calculating the inflow angle:

$$\phi = \tan^{-1}\left(\frac{U_\infty(1-a)}{\omega r\,(1+a')\cos(\Lambda-\zeta)}\right) \tag{4}$$

where a and a' are the axial and tangential induction factors, respectively. The angle of attack, which is a two-dimensional quantity defined in the direction of the airfoil orientation, is then given by

$$\alpha = \phi - \beta \tag{5}$$

Secondly, when discussing blade loading, it is relevant to distinguish between forces per unit blade length and per unit radius. In contrast to a straight blade, there are non-negligible differences between the two for swept blades (Madsen et al., 2020). The infinitesimal blade length $\mathrm{d}l$, oriented along the local blade axis, is related to the infinitesimal radial coordinate $\mathrm{d}r$ by

$$\mathrm{d}l\,\cos(\Lambda-\zeta) = \mathrm{d}r \tag{6}$$

3 Results

This section presents the results of the conducted wind tunnel campaign. Section 3.1 details the encountered challenge of varying pitch offsets and twist deformations between the three blades. The primary collected data, namely the flow fields are presented in Section 3.2, while derived blade-level aerodynamics and the lift coefficients are presented in Sections 3.3 and 3.4, respectively.[EF]

3.1 Determination of the combined pitch and twist offset

As mentioned in Section 2.1, the blades were manufactured out of vacuum-infused carbon fibre-reinforced material. The manual manufacturing can lead to minor differences in the exact positioning of the carbon fibre layers for the individual blades. On top of that, the resin infusion can introduce changes to the layup, which are much more difficult to mitigate as the blade moulds are closed during this process. As a consequence, varying twist deformations occurred for the three blades during operation.~~The blades used in this experiment were manually manufactured out of vacuum-infused carbon fibre-reinforced material. Despite being manufactured to be stiff, it is expected that blade sweep introduces twist deformations. Experience from previous experiments taught that the stiffness properties of the three blades can vary considerably (Fritz et al., 2024)~~[EF] Additionally, a manual pitch mechanism implemented between the blade root and hub led~~can lead~~[EF] to minor pitch offsets.

To quantify the pitch/twist offsets, the blade cross-sections visible in the raw images were inspected and compared against the original blade design. This approach is visualised in Figure 5 (a), showing a blade cross-section illuminated in white and the original design, i.e. the expected airfoil orientation,[EF] overlaid in red. In green, the corrected airfoil orientation is shown, generated by rotating the original design around the trailing edge until it approximately aligns with the pressure side of the illuminated cross-section.

It should be noted that for a measurement point in the unswept region of the blade, this orientation correction corresponds directly to a deviation from~~correction of~~[EF] the original twist distribution and pitch angle. For measurement planes in the swept part of the blade, this correction is less trivial, as the visible cross-section corresponds approximately to the local airfoil elongated vertically by a factor of $1/\cos(\Lambda - \zeta)$, see Figure 4. Therefore, the deviation from~~correction to~~[EF] the twist distribution, determined in the measurement plane, has to be multiplied with the same factor to correct the twist in the airfoil coordinate system. Figure 5 (b) shows the resulting offset in twist/pitch from the original design.

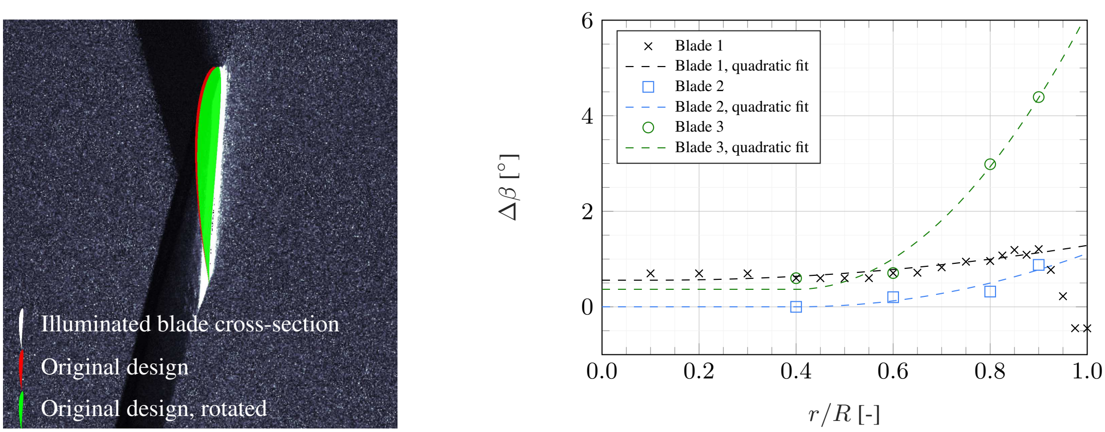

(a) (b)

Figure 5. Approach of determining actual local airfoil orientation (a), twist/pitch offset determined by comparing experimentally captured blade cross-sections to the original design (b)

For all blades, a quadratic curve is fitted to the distribution of pitch/twist offset to balance out fluctuations, likely due to human error in interpreting the raw images. This is particularly evident in~~true for~~[EF] the tip measurements of blade 1:~~, where~~[EF] the very small chord makes the interpretation of the cross-section's orientation difficult. Thus, measurements with $r/R > 0.9$ were excluded in generating the curve fit. The mathematical description of~~equations describing~~[EF] the quadratic curve fits are given in Equations (7a) – (7c)~~Table ??~~[EF]. All three blades exhibit twisting behaviour as expected for aft-swept blades, namely twisting to lower angles of attack under aerodynamic loading. However, the three blades vary significantly in their twist extent. The tip twist deformation angle varies from $\Delta\beta(r=R)-\Delta\beta(r=0)=0.7°$ ~~$\Delta\beta_{tip-root}=0.7°$~~[EF] for blade 1 to $\Delta\beta(r=R)-\Delta\beta(r=0)=1.1°$ ~~$\Delta\beta_{tip-root}=1.1°$~~[EF] for blade 2 and $\Delta\beta(r=R)-\Delta\beta(r=0)=5.8°$ ~~$\Delta\beta_{tip-root}=5.8°$~~[EF] for blade 3. While the blade deformations and pitch offsets were unintentional, the method described here allows the determination of the actual blade geometries with reasonable accuracy. This bears significance for potential future numerical validation studies based on the experimental results presented in the following sections.

$$\Delta\beta_{Blade\ 1}=\begin{cases}0.5580 & \text{for } r/R\leq 0.1\\ 1.1090\,(r-0.1\,R)^2+0.5580 & \text{for } r/R>0.1\end{cases} \tag{7a}$$

$$\Delta\beta_{Blade\ 2}=\begin{cases}0.0008 & \text{for } r/R\leq 0.4\\ 3.8330\,(r-0.4\,R)^2+0.0008 & \text{for } r/R>0.4\end{cases} \tag{7b}$$

$$\Delta\beta_{Blade\ 3}=\begin{cases}0.3662 & \text{for } r/R\leq 0.4\\ 19.8100\,(r-0.4\,R)^2+0.3662 & \text{for } r/R>0.4\end{cases} \tag{7c}$$

[EF]

3.2 Flow field

The PIV-processed velocity fields are the primary data collected during this experiment. V~~Non-dimensionalised v~~[EF]elocity magnitudes from the measurement planes where data from all three blades is available are shown in Figure 6 non-dimensionalised by the local relative inflow velocity, which is defined as[EF]

$$V_{rel}=\sqrt{(U_\infty(1-a))^2+(\omega\,r\,(1+a')\,\cos(\Lambda-\zeta))^2} \tag{8}$$

[EF]

The induction terms used in this equation are presented in the next section.[EF]

The general flow patterns are congruent between the three blades. Yet, differences caused by the varying pitch/twist offsets from the original blade design are evident from the flow fields, see e.g., the second row of subplots corresponding to $r/R=0.6$. Blade 2, experiencing the highest angle of attack of all three blades, exhibits higher induced velocities and, thus, higher velocity magnitudes on the suction side. By contrast, blade 3 twists to lower angles of attack, entailing lower velocity magnitudes in the blade's vicinity.

Close to the suction side, low-velocity regions are observable for many measurement points. These are caused by laser reflection from the convex blade surface, complicating the PIV processing. They are much less prominent on the concave pressure side.

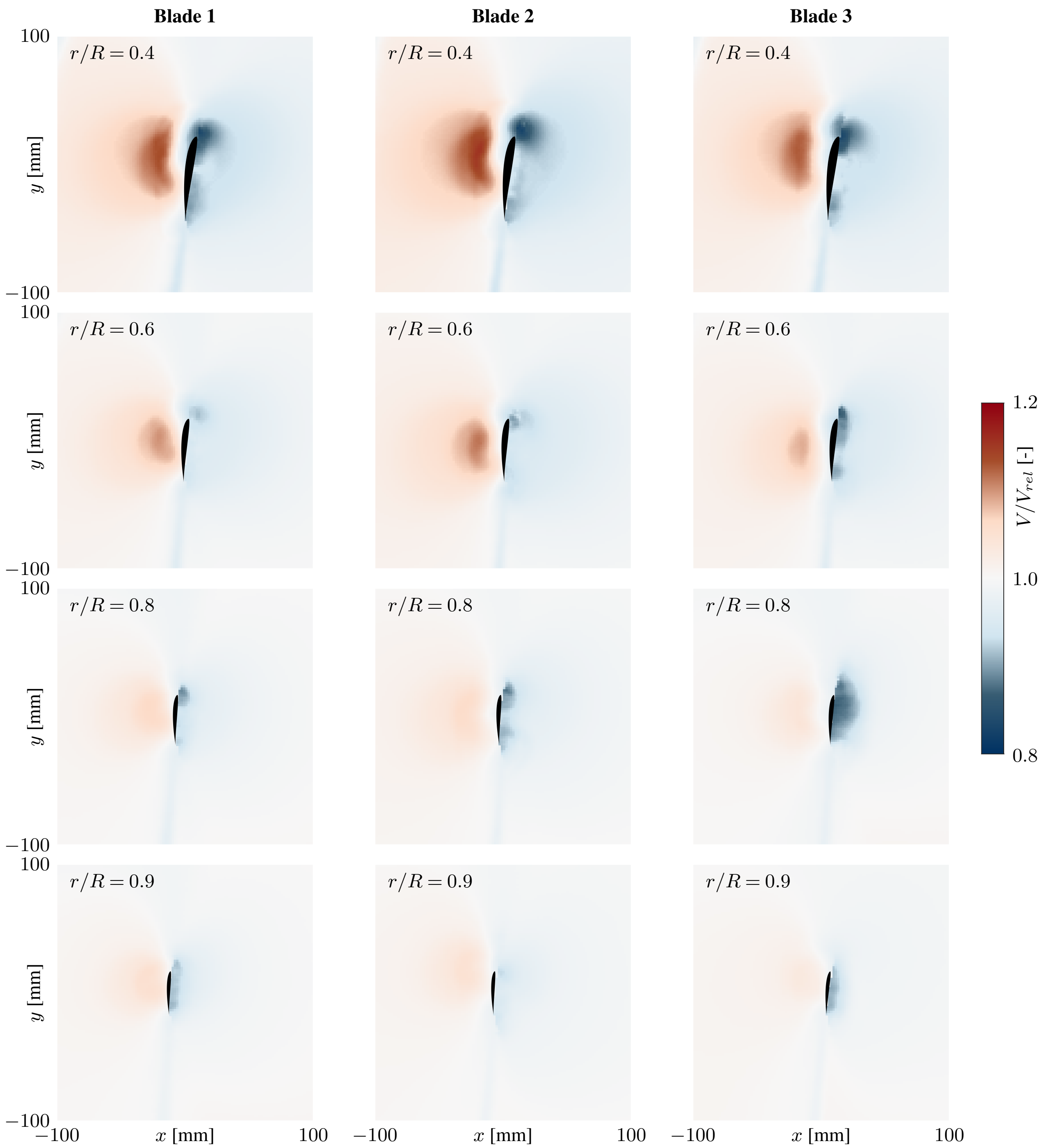

Figure 6. Non-dimensionalised velocity magnitudes at the radial stations measured for all three blades

3.3 Blade aerodynamics

This section discusses the spanwise distributions of the derived aerodynamic quantities. In addition to the mean value, error bars indicate the 95 % confidence interval based on the standard deviation in the measured velocity fields as calculated during the PIV processing. This uncertainty covers both the accuracy of phase-locking and the variability of the flow field during the image acquisition. Noteworthy uncertainties are only present at the blade root. These can be attributed to reflections from the nacelle and hub, which lead to increased uncertainty in the PIV processing. In the outer regions, uncertainties are negligible, indicating very high accuracy in phase-locking and steady flow conditions. As a consequence, the error bars for these data points are smaller than the marker size of the mean value.[EF]

Figure 7 shows the circulation distribution of the three blades. Straight wind turbine blades are usually designed to have a constant circulation value over large parts of the blade in design conditions. This is also the case for the IEA 15 MW RWT, which served as a reference to develop the planform of the straight blades presented in Fritz et al. (2024). The presence of blade sweep leads to a slanted distribution with the circulation decreasing towards the tip. It is not clear how much of this ~~This~~[EF] can ~~partially~~[EF] be attributed to the misalignment of airfoil orientation and inflow velocity and how much~~partially~~[EF] to the bend twist coupling presented in Section 3.1. The differences in circulation distribution between the three blades align with the observed pitch/twist offset.

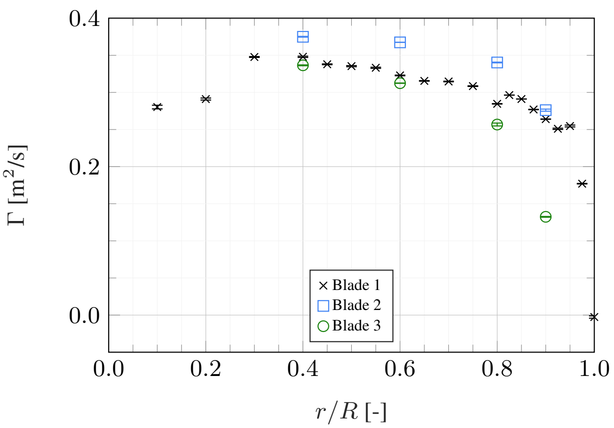

Figure 7. Spanwise distribution of bound circulation, error bars representing the 95% confidence interval

The axial and tangential induction factors are plotted in Figure 8. Both distributions exhibit relatively small differences between the three blades, with the only relevant deviations at $r/R = 0.9$ where the twist deformations vary strongly. A similar pattern was observed for the experimental campaign with straight blades (Fritz et al., 2024). It indicates that, at the rather high tip speed ratio present in this experiment, induction is largely a rotor-averaged phenomenon, independent of whether the blades are swept or not. At the tip, the axial induction reaches negative values. It can be speculated that this is due to the tip vortex's induction and that the three-dimensional nature of the flow in this region is also responsible for the slightly higher uncertainties present at this measurement location.

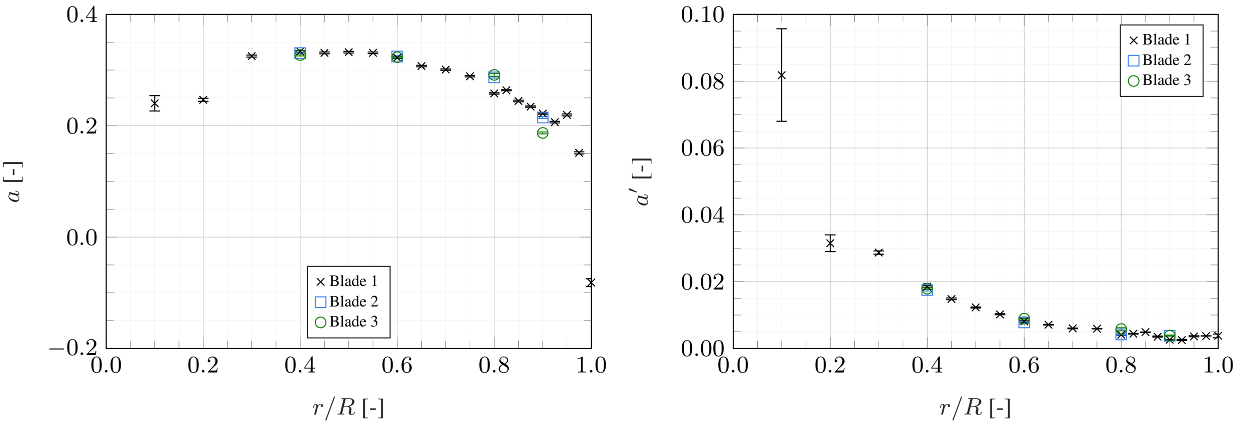

(a) (b)

Figure 8. Spanwise distribution of axial (a) and tangential (b) induction factors, error bars representing the 95% confidence interval

Figure 9 shows the inflow angle and angle of attack distribution, both quantities defined perpendicular to the local blade axis. At $r/R = 0.1$, the blade geometry is defined by a cylindrical cross-section, rendering the angle of attack value presented at this location meaningless. In line with the derived induction values, the inflow angle varies very little between the three blades. The angle of attack, however, is evidently influenced by each blade's pitch/twist offset. Particularly, blade 3, which has the highest twist deformations, experiences near-zero angles of attack at the tip. Given that the *SD7032* airfoil used in the blade design stalls at approximately $\alpha = 11°$ (Fontanella et al., 2021b), all angle of attack values derived from the PIV data suggest operation in the linear region of the airfoil.

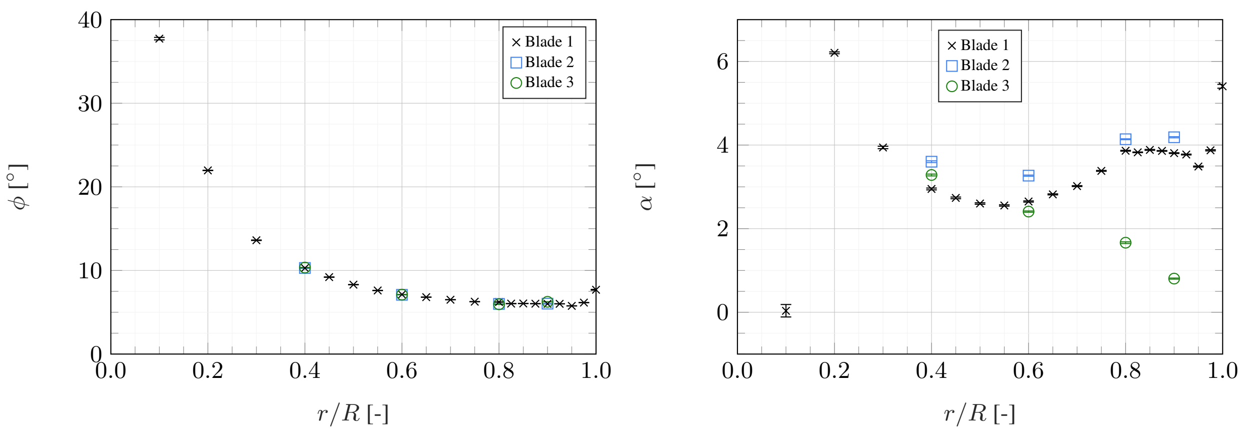

(a) (b)

Figure 9. Spanwise distribution of inflow angle (a) and angle of attack (b), error bars representing the 95% confidence interval

The normal and tangential force distribution is depicted in Figure 10. It should be noted that the forces are given per unit radius and not per unit blade length. This corresponds to the forces in the coordinate system spanning the measurement planes and, thus, not in the plane of the airfoil definition (see Figure 4)[EF]. The normal force is calculated using both Noca's method as well as the Kutta-Joukowski theorem (KJ). The rotor thrust can be calculated by integrating the normal force along the blade radius. For this purpose, piecewise cubic curves are fit to the experimental data with zero loading prescribed at root and tip if no data is available there. The non-dimensionalisation of the rotor thrust yields the thrust coefficient $C_T = F_N / \left(0.5\rho U_\infty^2 \pi R^2\right)^{-1}$ $C_T = \frac{F_N}{0.5\rho U_\infty^2 \pi R^2}$[EF]. Depending on the approach, the experimental thrust coefficients are $C_{T,Noca} = 0.7464$ and $C_{T,KJ} = 0.7044$, respectively.

Fritz et al. (2024) demonstrated for a comparable dataset that Noca's method does not converge with varying control volume size for the tangential force; the same holds for the data presented in this study, which is why only the tangential force calculated using Kutta-Joukowski theorem is presented here. With the exception of the measurements at $r/R = 0.2$, Noca's method consistently results in slightly higher normal force values than the Kutta-Joukowski theorem. Variations in the calculated forces are, again, aligned with the pitch/twist offset discussed above.

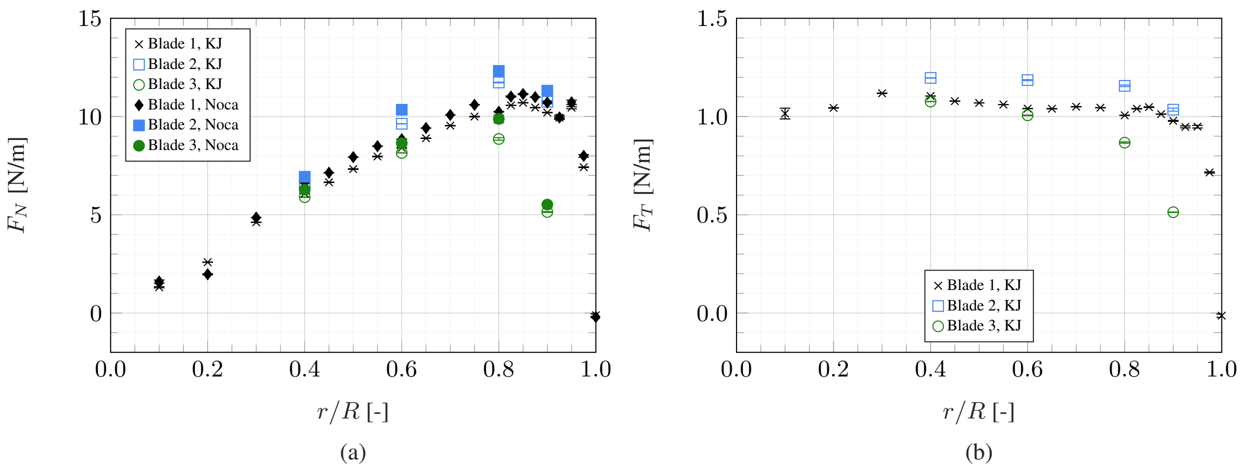

Figure 10. Spanwise distribution of normal (a) and tangential (b) force, error bars representing the 95% confidence interval

3.4 Lift polar

Given the aerodynamic characteristics presented in the previous section, the experimental lift coefficient c_l can be calculated for each measurement point. Being an airfoil-level quantity, the lift coefficient has to be calculated using quantities aligned with the airfoil orientation. Using Equation 6, the forces measured per unit radius can be converted to forces per unit blade length, so that

$$c_l = \frac{F_{N,KJ}\cos(\Lambda-\zeta)\cos(\phi) + F_{T,KJ}\cos(\Lambda-\zeta)\sin(\phi)}{\frac{1}{2}\rho V_{rel}^2 c} \quad (9)$$

where ρ is the density of air~~ and $V_{rel} = \sqrt{(U_\infty(1-a))^2 + (\omega r(1+a')\cos(\Lambda-\zeta))^2}$ is the relative inflow velocity in the airfoil plane~~[EF]. The resulting values are plotted in Figure 11 (a)[EF] alongside the *SD7032* lift polar (Fontanella et al., 2021b) at Reynolds numbers resembling~~at a chord Reynolds number of $Re_c = 60000$, which resembles~~[EF] the experimental conditions varying between approximately[EF] 40000 and 70000 along the blade span. The two measurement points closest to the root and the two closest to the tip are omitted. At the root, the blade is not defined by the design airfoil but rather by a cylinder and a blend between cylinder and airfoil. At the tip, the tip vortex increases the flow's three-dimensionality and thus, measurements cannot be compared to two-dimensional wind tunnel data. For all other measurement points, the agreement between the design airfoil's lift polar and the experimental values is good.

While Figure 11 (a) provides insight into the experimentally obtained lift polar, it lacks representation of the varying Reynolds number across the blade. Alternatively, the experimentally derived lift coefficient c_l is plotted as a function of the radial position alongside the chord Reynolds number distribution in Figure 11 (b). Additionally, the design airfoil polars can be evaluated for the experimentally derived angle of attack and Reynolds number to obtain the expected polar-based lift coefficient $c_{l,pol}$. Comparing c_l and $c_{l,pol}$ reveals that blades 1 and 2 utilised in this experiment generate less lift than anticipated in the outboard regions. The experimentally derived lift coefficient of blade 3 agrees well with the expected polar-based one. It can be hypothesised that this discrepancy can be attributed to differences in surface finish between the model blades and the airfoil studied by Fontanella et al. (2021a) and minor inaccuracies in the manually manufactured geometry. The latter have a more significant impact towards the tip where the chord values are very low.[EF]

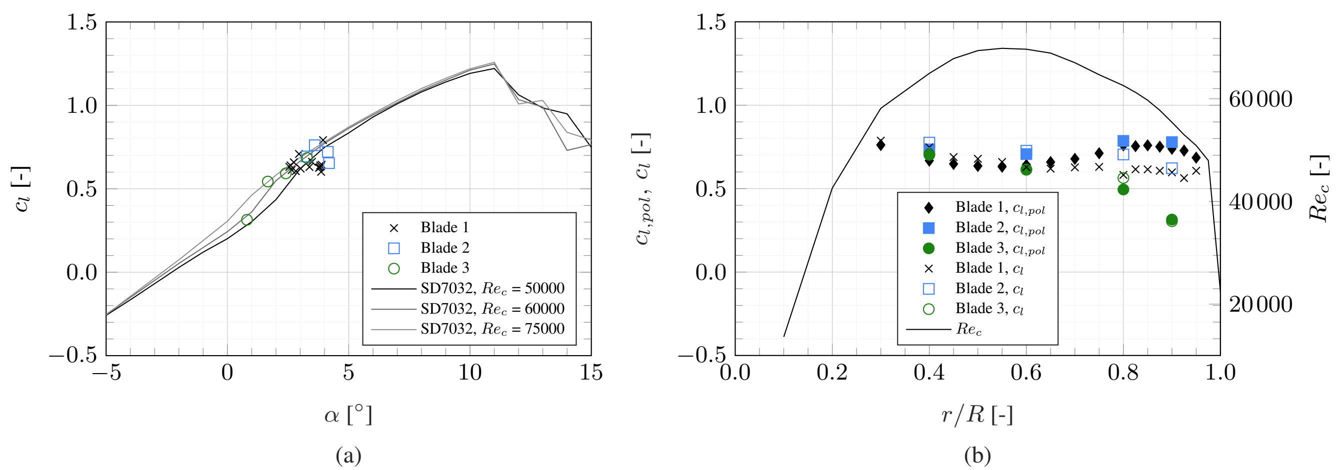

Figure 11. Experimental lift polar~~coefficient~~[EF] compared to the *SD7032* airfoil lift polar (a) and comparison between the lift coefficient derived from measured forces to that expected based on the design lift polars, alongside the chord Reynolds number distribution (b)[EF]

4 Conclusions and outlook

This study presents results from a wind tunnel experiment where a three-bladed model turbine equipped with swept blades was tested. The velocity fields around multiple radial stations were measured using a Particle Image Velocimetry setup. From the measured velocity fields, blade-level aerodynamic quantities are derived, namely bound circulation, induction values, inflow angle and angle of attack, and forces normal and tangential to the rotor plane. The normal force distributions, determined with both Noca's method and the Kutta-Joukowski theorem, agree reasonably well. Furthermore, the deviations in the aerodynamic response[EF] between the three blades are consistent with the determined offsets in blade pitch and twist deformations from the original design. Knowing the aerodynamic blade characteristics, the local lift coefficient can be calculated, which shows good agreement with the lift polar of the design airfoil.

The created dataset characterises the three swept blades aerodynamically in rotating and controlled conditions. Such data, rarely available even for more conventional straight blades, was absent in the current literature. It provides a baseline for future experimental research on the same model turbine as well as a valuable validation dataset for numerical tools of varying fidelity aiming at simulating swept wind turbine blades. While the flow fields can serve for the validation of higher fidelity models, such as panel codes and computational fluid dynamics, the blade-level aerodynamics are also relevant to lower fidelity models, such as BEM and lifting line algorithms.

In future research, it is intended to use the experimental results presented here to validate the BEM correction model for swept blades developed by Fritz et al. (2022). This validation exercise gains in importance due to the pitch/twist offsets experienced in this experiment and the one presented in Fritz et al. (2024). The two campaigns were designed to deliver datasets enabling a direct comparison of straight and swept blade aerodynamics. Since pitch offsets and blade deflections varied considerably between the three blades and even more so between the two campaigns, such a direct comparison now requires an approach to accurately correct both datasets for these offsets. It is expected that once the BEM correction model is validated, it can be used to correct the experimental datasets and facilitate the intended comparison.

Data availability. The data presented in this study, as well as information regarding the blade planform and logged wind tunnel operating conditions, are openly available on the 4TU.ResearchData repository at DOI:10.4121/c9631f69-8855-4e2d-8777-38338534b4ea.

Appendix A: Nomenclature

Latin letters

a, a'	Axial and tangential induction factor
C_T	Thrust coefficient
c	Chord
c_l	Lift coefficient
D	Rotor diameter
F_N, F_T	Normal and tangential force
l	Coordinate along blade axis
R	Blade tip radius
Re_c	Chord Reynolds number
r	Radial coordinate
r_{start}	Sweep starting position
t	Time
U_∞	Free stream velocity
V_{rel}	Relative inflow velocity
y_Λ	Blade sweep
y_{tip}	Tip sweep extent

Greek letters

α	Angle of attack
β	Combined blade pitch and twist angle
γ	Sweep exponent
Γ	Circulation
ζ	Global sweep angle
Λ	Local sweep angle
λ	Tip speed ratio
ρ	Density of air
ϕ	Inflow angle
ω	Angular velocity

Subscripts

KJ	Kutta-Joukowski
pol	Based on design polars

Appendix B: Measurement plane locations[EF]

Table B1 gives an overview of the measurement planes. Here, y is the coordinate lateral to the inflow direction measured from the rotor centre. At planes that are marked as "All blades", measurements were taken for blades 1, 2 and 3, while only blade 1 was measured at all other planes.[EF]

Author contributions. EF designed the wind turbine model, built the model blades, planned and executed the experiment, and post-processed and analysed the measurement data. KB acquired funding and contributed to the experiment planning and the data analysis. CF acquired funding and contributed to the experiment planning and execution, the development of post-processing methods, and the data analysis.

Competing interests. The authors declare that they have no competing interests.

Plane	r/R [-]	y [mm]	All blades
1	0.100	90.0	
2	0.200	180.0	
3	0.300	270.0	
4	0.400	360.0	×
5	0.450	405.0	
6	0.500	450.0	
7	0.550	495.0	
8	0.600	540.0	×
9	0.650	585.0	
10	0.700	630.0	
11	0.750	675.0	
12	0.800	720.0	×
13	0.825	742.5	
14	0.850	765.0	
15	0.875	787.5	
16	0.900	810.0	×
17	0.925	832.5	
18	0.950	855.0	
19	0.975	877.5	
20	1.000	900.0	
21	1.025	922.5	
22	1.050	945.0	

Table B1. Overview of the measurement planes

Acknowledgements. This contribution has been financed with Topsector Energiesubsidie from the Dutch Ministry of Economic Affairs under grant no. TEHE119018. The wind tunnel experiment was financed by internal TU Delft funding.

References

Anderson, J. D.: Fundamentals of aerodynamics, McGraw-Hill series in aeronautical and aerospace engineering, McGraw-Hill Education, New York, NY, sixth edn., 2017.

Ashwill, T., Kanaby, G., Jackson, K., and Zuteck, M.: Development of the sweep-twist adaptive rotor (STAR) blade, in: 48th AIAA aerospace sciences meeting including the new horizons forum and aerospace exposition, American Institute of Aeronautics and Astronautics, https://doi.org/10.2514/6.2010-1582, 2010.

Barlas, T., Pirrung, G. R., Ramos-García, N., Horcas, S. G., Mikkelsen, R. F., Olsen, A. S., and Gaunaa, M.: Wind tunnel testing of a swept tip shape and comparison with multi-fidelity aerodynamic simulations, Wind Energy Science, 6, 1311–1324, https://doi.org/10.5194/wes-6-1311-2021, publisher: Copernicus GmbH, 2021.

Barlas, T., Pirrung, G. R., Ramos-García, N., González Horcas, S., Li, A., and Madsen, H. A.: Atmospheric rotating rig testing of a swept blade tip and comparison with multi-fidelity aeroelastic simulations, Wind Energy Science, 7, 1957–1973, https://doi.org/10.5194/wes-7-1957-2022, publisher: Copernicus GmbH, 2022.

Fontanella, A., Bayati, I., Mikkelsen, R., Belloli, M., and Zasso, A.: UNAFLOW: a holistic wind tunnel experiment about the aerodynamic response of floating wind turbines under imposed surge motion, Wind Energy Science, 6, 1169–1190, https://doi.org/10.5194/wes-6-1169-2021, publisher: Copernicus GmbH, 2021a.

Fontanella, A., Bayati, I., Mikkelsen, R., Belloli, M., and Zasso, A.: UNAFLOW: UNsteady Aerodynamics of FLOating Wind turbines, https://doi.org/10.5281/zenodo.4740006, 2021b.

Fontanella, A., Facchinetti, A., Di Carlo, S., and Belloli, M.: Wind tunnel investigation of the aerodynamic response of two 15 MW floating wind turbines, Wind Energy Science, 7, 1711–1729, https://doi.org/10.5194/wes-7-1711-2022, publisher: Copernicus GmbH, 2022.

Fritz, E., Ribeiro, A., Boorsma, K., and Ferreira, C.: Aerodynamic characterisation of a thrust-scaled IEA 15 MW wind turbine model: experimental insights using PIV data, Wind Energy Science, 9, 1173–1187, https://doi.org/10.5194/wes-9-1173-2024, 2024.

Fritz, E. K., Ferreira, C., and Boorsma, K.: An efficient blade sweep correction model for blade element momentum theory, Wind Energy, 25, 1977–1994, https://doi.org/10.1002/we.2778, 2022.

Gaertner, E., Rinker, J., Sethuraman, L., Zahle, F., Anderson, B., Barter, G., Abbas, N., Meng, F., Bortolotti, P., Skrzypinski, W., Scott, G., Feil, R., Bredmose, H., Dykes, K., Shields, M., Allen, C., and Viselli, A.: Definition of the IEA wind 15-megawatt offshore reference wind turbine Tech. Rep., 2020.

Kimball, R., Robertson, A., Fowler, M., Mendoza, N., Wright, A., Goupee, A., Lenfest, E., and Parker, A.: Results from the FOCAL experiment campaign 1: turbine control co-design, Journal of Physics: Conference Series, 2265, 022 082, https://doi.org/10.1088/1742-6596/2265/2/022082, publisher: IOP Publishing, 2022.

Larwood, S. and Zuteck, M.: Swept wind turbine blade aeroelastic modeling for loads and dynamic behavior, AWEA Windpower, 2006.

Larwood, S., van Dam, C., and Schow, D.: Design studies of swept wind turbine blades, Renewable Energy, 71, 563–571, https://doi.org/10.1016/j.renene.2014.05.050, publisher: Elsevier BV, 2014.

Li, A., Pirrung, G., Madsen, H. A., Gaunaa, M., and Zahle, F.: Fast trailed and bound vorticity modeling of swept wind turbine blades, Journal of Physics: Conference Series, 1037, 062 012, https://doi.org/10.1088/1742-6596/1037/6/062012, publisher: IOP Publishing, 2018.

Li, A., Gaunaa, M., Pirrung, G. R., Ramos-García, N., and Horcas, S. G.: The influence of the bound vortex on the aerodynamics of curved wind turbine blades, Journal of Physics: Conference Series, 1618, 052 038, https://doi.org/10.1088/1742-6596/1618/5/052038, publisher: IOP Publishing, 2020.

Li, A., Pirrung, G. R., Gaunaa, M., Madsen, H. A., and Horcas, S. G.: A computationally efficient engineering aerodynamic model for swept wind turbine blades, Wind Energy Science, 7, 129–160, https://doi.org/10.5194/wes-2021-96, publisher: Copernicus GmbH, 2021.

Liebst, B. S.: Wind turbine gust load alleviation utilizing curved blades, Journal of Propulsion and Power, 2, 371–377, https://doi.org/10.2514/3.22897, publisher: American Institute of Aeronautics and Astronautics (AIAA), 1986.

Madsen, H. A., Larsen, T. J., Pirrung, G. R., Li, A., and Zahle, F.: Implementation of the blade element momentum model on a polar grid and its aeroelastic load impact, Wind Energy Science, 5, 1–27, https://doi.org/10.5194/wes-5-1-2020, 2020.

Noca, F., Shiels, D., and Jeon, D.: A comparison of methods for evaluating time-dependant fluid dynamic forces on bodies, using only velocity fields and their derivatives, Journal of Fluids and Structures, 13, 551–578, https://doi.org/10.1006/jfls.1999.0219, 1999.

Pirrung, G. R., Madsen, H. A., Kim, T., and Heinz, J.: A coupled near and far wake model for wind turbine aerodynamics, Wind Energy, 19, 2053–2069, https://doi.org/10.1002/we.1969, publisher: Wiley, 2016.

Rahimi, H., Schepers, J., Shen, W., García, N. R., Schneider, M., Micallef, D., Ferreira, C. S., Jost, E., Klein, L., and Herráez, I.: Evaluation of different methods for determining the angle of attack on wind turbine blades with CFD results under axial inflow conditions, Renewable Energy, 125, 866–876, https://doi.org/10.1016/j.renene.2018.03.018, 2018.

Schepers, G.: IEA Task 47 Innovative aerodynamic experiment technologies and simulations on wind turbines in turbulent inflow, https://zenodo.org/doi/10.5281/zenodo.4580358, 2021.

Suzuki, K., Schmitz, S., and Chattot, J.-J.: Analysis of a swept wind turbine blade using a hybrid Navier–Stokes/Vortex-Panel model, in: Computational fluid dynamics 2010, pp. 213–218, Springer Berlin Heidelberg, https://doi.org/10.1007/978-3-642-17884-9_25, 2011.

Verelst, D. R. and Larsen, T. J.: Load consequences when sweeping blades - A case study of a 5 MW pitch controlled wind turbine, Tech. Rep. RISO-R-1724(EN), Technical University of Denmark, Risø National Laboratory for Sustainable Energy. Wind Energy Division, Roskilde (Denmark), 2010.